

# Electrical Properties of Graphene/AlGa<sub>N</sub>/Ga<sub>N</sub> Heterostructures

Pil Sung Park<sup>1a)</sup>, Kongara M. Reddy<sup>2</sup>, Digbijoy N. Nath<sup>1</sup>, Nitin P. Padture<sup>3</sup> and Siddharth Rajan<sup>1,2</sup>

<sup>1</sup>Electrical Engineering Department, The Ohio State University, Columbus, OH 43210, USA

<sup>2</sup>Department of Materials Science and Engineering, The Ohio State University, Columbus, OH 43210, USA

<sup>3</sup>School of Engineering, Brown University, Providence, RI 02912, USA

***Abstract***— We report on the electrical properties of graphene/AlGa<sub>N</sub>/Ga<sub>N</sub> heterostructures using lateral graphene field-effect-transistors (FETs) and vertical metal-graphene-AlGa<sub>N</sub>-Ga<sub>N</sub> diodes. From a comparison with graphene FETs on SiO<sub>2</sub>, it is found that a significant carrier mobility degradation is caused at the graphene/AlGa<sub>N</sub> interface which we attribute to fixed charges which neutralize polarization sheet charges at the AlGa<sub>N</sub> surface. Unexpectedly, the insertion of graphene between a metal and AlGa<sub>N</sub> was found to enable ohmic contact between the metal and semiconductor. This effect could be used as a simple manufacturable way to obtain ohmic contacts for high-electron-mobility-transistors (HEMTs.)

***Keywords***—large-area, CVD, graphene, FETs, GFETs, HEMTs, AlGa<sub>N</sub>/Ga<sub>N</sub>, tunneling, ohmic contacts

## 1. Introduction

Since the demonstration of graphene<sup>1,2</sup> and its zero band gap and unique bandstructure, several exciting properties such as ultrahigh carrier mobility<sup>3,4</sup>, record-breaking strength<sup>5</sup>, electrochemical

---

a) Author to whom correspondence should be sent: Pil Sung Park, email: [parkp@ece.osu.edu](mailto:parkp@ece.osu.edu), Tel: 001-614-329-3712

stability<sup>6</sup>, etc. have been demonstrated. Moreover, as a result of the availability of high-quality and large-scale graphene synthesis<sup>7</sup> or epitaxial growth<sup>8</sup>, graphene-based applications can be adopted onto any kinds of surface<sup>9</sup>. However, a high-quality substrate is necessary to minimize external perturbations for exploiting the maximum capability of graphene electronics<sup>10</sup>. It was shown using hexagonal boron-nitride (hBN)<sup>11</sup> that other group III-nitride material-based substrates also can be good candidates, since they have high breakdown characteristics<sup>12</sup>, high phonon energy<sup>13</sup>, high thermal conductivity<sup>14</sup> and electrochemical stability<sup>15</sup>. In this paper, we investigate graphene/AlGaIn/GaN heterostructures where a two-dimensional-electron-gas (2DEG) is formed at the AlGaIn and GaN hetero-interface, and show that graphene can be used to create excellent ohmic contact to the 2DEG without the ohmic annealing or regrowth techniques that are used currently. In addition, these results extend the understanding of 2D/3D semiconductor junctions.

## **2. Material and substrate preparation**

We transferred CVD-grown graphene onto Si/SiO<sub>2</sub> and AlGaIn/GaN substrates for this experiment. Monolayer graphene films were grown on high purity polycrystalline Cu foils (Alfa Aesar, Ward Hill, MA) of 25 $\mu$ m thickness with following process. Cu foils of the size of 1  $\times$  1 cm<sup>2</sup> were placed into the chemical-vapor-deposition (CVD) chamber consisting of a controlled-atmosphere quartz-tube furnace (Lindberg/Blue M, Asheville, NC). Then, the chamber was evacuated to a base pressure of 20 mTorr, and purged out with H<sub>2</sub> under a set pressure of 250mTorr. After purging, H<sub>2</sub> flux was changed to 10 sccm, and the chamber was heated up to 1000  $^{\circ}$ C and maintained for 20 min to stabilize the Cu foil at the temperature. High-purity CH<sub>4</sub> (35 sccm) was then introduced, simultaneously, and the graphene layer was synthesized for 25 min under the final chamber pressure of 700 mTorr (H<sub>2</sub> + CH<sub>4</sub>).

Using Polymethyl methacrylate (PMMA) method<sup>7</sup>, the graphene film was transferred onto an AlGaIn/GaN heterostructure which was grown on Fe-doped semi-insulating GaN on Sapphire substrate (Lumilog, Vallauris, France) at  $\sim$  770  $^{\circ}$ C by plasma-assisted molecular-beam-epitaxy (Veeco Gen 930,

Plainview, NY). Fig. 1 (a) shows the material characteristics of AlGaN/GaN substrate. The thickness and Al-composition of AlGaN barrier were found to be 31 nm and 28% from XRD measurement. And the RMS roughness of 0.5 nm was measured from AFM measurement on AlGaN surface which is comparable to thermally grown SiO<sub>2</sub> layer (typical surface roughness of SiO<sub>2</sub> < 1 nm). To compare the performance of graphene FETs, the graphene film was also transferred onto SiO<sub>2</sub> (300nm)/Si substrate (SQI, San Jose, CA).

The transferred graphene films on AlGaN/GaN and SiO<sub>2</sub> substrates were characterized by Raman spectroscopy (InVia Raman Microscope, Renishaw, Gloucestershire, U.K.) using a laser with 514 nm wavelength and 1mW power. Spectra of 10 scans on each spot were collected and averaged for numerous locations. Fig. 1 (b) depicts representative Raman spectra from transferred graphene layer on each substrate. The spectra of each graphene layer showed well-known D-band, G-band, and 2D-band peaks near 1350 cm<sup>-1</sup>, 1580 cm<sup>-1</sup>, and 2700 cm<sup>-1</sup>, respectively. And the approximate 2D:G peak ratios of 2:1, indicative of the number of graphene layer, confirmed that the transferred graphene film is monolayer.

### 3. Device Fabrication

Graphene FETs (Fig. 2 (a)) and metal-graphene-semiconductor (M-G-S) diodes (Fig.2 (b)), were fabricated on the AlGaN/GaN substrate. To compare characteristics, graphene FETs on SiO<sub>2</sub> and metal-semiconductor Schottky diodes on AlGaN/GaN substrate were also processed together. E-beam evaporated Cr/Au/Ni ohmic contacts were formed using photolithography and lift-off process, followed by the mesa isolation using O<sub>2</sub> plasma reactive-ion-etching. E-beam evaporated and oxidized AlO<sub>x</sub> and atomic layer deposited (ALD) Al<sub>2</sub>O<sub>3</sub> were stacked for the top-gate dielectric. Finally, 20 μm-long gate with Ni/Au/Ni metal stack was defined to minimize the parasitic resistance from the metal-graphene contacts, and the source- and drain-access regions, i.e. the channel resistance measured for the field-effective mobility calculation dominates the measured total resistance. The FETs had a width of 100 μm, gate length of 20 μm, gate-source and gate-drain spacing of 2 μm. The same metal stack (Cr/Au/Ni)

used for the ohmic contacts on graphene FETs were also used on metal-graphene-semiconductor and metal-semiconductor junction diodes, while the metal-semiconductor junction diode was formed by simply removing graphene layer using O<sub>2</sub> plasma RIE before metal-evaporation. The ohmic contact to the 2DEG in GaN was formed at the edge of the sample using pressed indium contacts.

#### 4. Results and discussion

DC measurements were carried out using an Agilent parameter analyzer B1500. Fig. 3 depicts the transfer characteristics ( $I_{DS}$ - $V_{GS}$ ) and  $\mu_{FE}$ - $V_{GS}$  characteristics of graphene FETs on AlGa<sub>N</sub>/Ga<sub>N</sub> and SiO<sub>2</sub> substrates at room temperature and atmospheric pressure. The Dirac-point on each substrate was found at  $V_{GS} = 1.2$  V, and  $V_{GS} = 1.6$  V for graphene on AlGa<sub>N</sub>/Ga<sub>N</sub> and SiO<sub>2</sub> substrates, respectively. From the Dirac-point shift, the graphene layers on both substrates were found to be p-doped. The variation of Dirac-point on different substrates is caused by the doping variation due to the interaction between graphene and substrate, and causes the difference in the drain current density at zero gate bias. The field-effective mobility,  $\mu_{FE}$ , was extracted from the calculated transconductance,  $g_m$ , and the measured capacitance-voltage (C-V) characteristics as

$$\mu_{FE} = \frac{L}{W} \cdot \frac{g_m(V_{GS})}{C(V_{GS})} \cdot \frac{1}{V_{DS}}$$

where  $g_m(V_{GS}) = dI_{DS}/dV_{GS}$  is calculated from measured transfer-characteristics,  $C(V_{GS})$  was directly measured on the gate pad of the transistor. The extracted  $\mu_{FE}$  of both FETs includes extrinsic resistances of metal-graphene contact, and source- and drain-access regions. Since the carriers in the access region remain p-type while the channel is modulating,  $\mu_{FE}$  shows enhanced hole mobility than electron mobility. The maximum electron and hole mobilities were found to be 14 cm<sup>2</sup>/V s and 33 cm<sup>2</sup>/V s for graphene on AlGa<sub>N</sub>/Ga<sub>N</sub> substrate, and 56 cm<sup>2</sup>/V s and 180 cm<sup>2</sup>/V s for graphene on SiO<sub>2</sub> substrate, respectively. This significant carrier mobility degradation can be explained with the electron mobility degradation of Ga<sub>N</sub> metal-oxide-semiconductor (MOS) structure due to a high interface charge density, at the graphene/Ga<sub>N</sub> interface<sup>17</sup> which can be understood from the intrinsic polarization properties of the

III-nitride system<sup>20</sup>. Polarization charges at the AlGaN surface are neutralized by randomly distributed surface fixed charges, attributed to defects, which affect electrons and holes through Coulomb scattering. This high charge density, of the order of  $10^{13}$  /cm<sup>3</sup>, which is more than one order higher magnitude of one for graphene/SiO<sub>2</sub> interface, makes Coulomb scattering the dominant scattering mechanism<sup>19</sup>. This effect is expected to occur on other substrates with strong polarization effects such as ZnO and CdS.

Top-down I-V characteristics of metal-graphene-semiconductor junction and metal-semiconductor junction diodes are depicted in Fig 5. (a). Cr ( $\Phi_{Cr} = 4.37$  eV) was selected to minimize the doping in graphene ( $\Phi_{Graphene} = 4.5$ eV) under metal contact, and forms  $\sim 1$  eV of Schottky barrier height,  $\Phi_B$ , on bare AlGaN interface. Although graphene with Cr contact is supposed to have a similar  $\Phi_B$  on AlGaN surface after band line up with Cr, *linear current characteristics in both forward and reverse bias* was observed in the M-G-S junction. To confirm the measured I-V characteristics are not a thermionic emission, both M-G-S diode and M-S diode were measured at low temperature (77 K  $\sim$  300 K) and low pressure ( $1 \sim 2 \times 10^{-6}$  Torr) (in Fig. 4 (a)-(b)). Unlike the M-S diode, which shows more than an order magnitude of difference in subthreshold and reverse-biased current density with temperature difference, the M-G-S diode shows a stable ohmic behavior in both low- and room-temperature conditions. Since  $\Delta E_C$  of 0.84 eV at Al<sub>0.3</sub>Ga<sub>0.7</sub>N/GaN hetero-interface should still impede forward tunneling even if a simple Fermi-level line-up between M-(G)-S junction forms 0 eV of  $\Phi_B$ , we compared this tunneling phenomenon with n-GaN(Si=6E19cm<sup>-3</sup>)/UID Al<sub>0.3</sub>Ga<sub>0.7</sub>N/n-GaN(Si=1E19cm<sup>-3</sup>). Though significant heterojunction barriers exist on both upper GaN/AlGaN and lower AlGaN/GaN heterointerfaces, a significant current in both forward and reverse direction was observed. This is in agreement with recent results on GaN/AlGaN/GaN structures where heterojunctions were found to have higher current density. In Figure 5(b), we show that the experimentally observed current density expected for n-GaN/30 nm Al<sub>0.3</sub>Ga<sub>0.7</sub>N/GaN structure is significantly higher than the theoretical tunneling or thermionic currents. A possible reason for the leakage is percolative transport through GaN or low Al composition regions of the

AlGaN. Since AlGaN is a random alloy, the “GaN-like” regions present minimal barrier to transport both from graphene to AlGaN in the graphene/AlGaN/GaN case and from GaN to AlGaN in the GaN/AlGaN/GaN case. This leads to an easy percolative path for transport between the graphene and the GaN. The lack of temperature dependence in the IV characteristics also point to such a mechanism. Another possibility for transport through the barrier, trap-mediated tunneling (Poole-Frenkel tunneling)<sup>21</sup> between the top and bottom layers is less likely since the observed current was independent of temperature.

Regardless of the mechanism, the observation of ohmic contact using graphene could have very important technological impact for AlGaN/GaN HEMTs. Currently, relatively complex methods such as high temperature annealing of metals or etching and regrowth are used to form ohmic contacts to the 2DEG at the AlGaN/GaN interface. Annealed ohmic contacts have edge roughness which puts minimum bounds of gate-source and gate-drain spacing, both of which need to be as small as possible for high frequency operation. On the other hand, etching and epitaxial regrowth increase the complexity of fabrication. The formation of ohmic contacts using graphene provides a simple and elegant solution to the problem.

## **5. Conclusion**

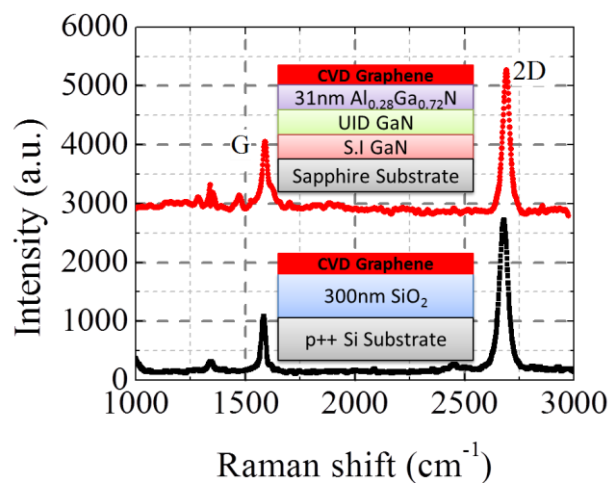
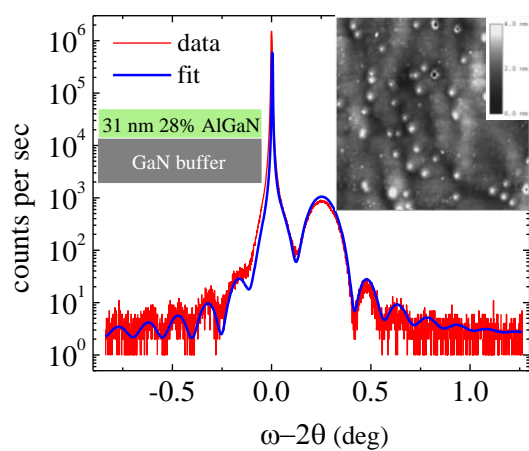
In summary, we have studied graphene-based devices on AlGaN/GaN substrates. A comparison of graphene FETs on AlGaN/GaN and SiO<sub>2</sub> substrates shows that un-mediated high interface charge density at AlGaN surface from intrinsic polarization effects leads a significant carrier mobility degradation due to Coulomb scattering. We also demonstrated unexpected ohmic behavior when a graphene sheet is inserted between metal and AlGaN/GaN layer. This provides a method to replace complicated ohmic contact forming processes in the fabrication process of HEMTs with a simple manufacturable process.

## Reference

1. K. S. Novoselov, A. K. Geim, S. V. Morozov, D. Jiang, M. I. Katsnelson, I. V. Grigorieva, S. V. Dubonos and A. A. Firsov, *Nature*, **438**, 197 (2005).
2. Y. Zhang, Y. Tan, H. L. Stormer and P. Kim, *Nature* **438**, 201 (2005).
3. X. Du, L. Skachko, A. Barker, and E. Y. Andrei, *Nat. Nanotechnol.* **3**, 491 (2008).
4. K. I. Bolotin, K. J. Sikes, Z. Jiang, M. Klima, G. Fudenberg, J. Hone, P. Kim, and H. L. Stormer, *Solid State Commun.* **146**, 351 (2008).
5. C. Lee, X. Wei, J. W. Kysar and J. Hone, *Science* **321**, 385 (2008)
6. L. Zhao, L. Zhao, Y. Xu, T. Qiu, L. Zhi, and G. Shi, *Electrochimica Acta* **55**, 491 (2009)
7. X. Li, W. Cai, J. An, S. Kim, J. Nah, D. Yang, R. Piner, A. Velamakanni, I. Jung, E. Tutuc, S. K. Banerjee, L. Colombo, R. S. Ruoff, *Science* **324**, 1312 (2009)
8. C. Berger, Z. Song, X. Li, X. Wu, N. Brown, C. Naud, D. Mayou, T. Li, J. Hass, A. N. Marchenkov, E. H. Conrad, P. N. First and W. A. de Heer. *Science* **312**, 1191 (2006)
9. S. Bae, H. Kim, Y. Lee, X. Xu, J. Park, Y. Zheng, J. Balakrishnan, T. Lei, H. R. Kim, Y. I. Song, Y. Kim, K. S. Kim, B. Özyilmaz, J. Ahn, B. H. Hong and S. Iijima, *Nat. Nanotechnol.* **5**, 574 (2010)
10. Y. Wu, K. A. Jenkins, A. Valdes-Garcia, D. B. Farmer, Y. Zhu, A. A. Bol, C. Dimitrakopoulos, W. Zhu, F. Xia, P. Avouris, and Y. Lin, *Nano Lett.* **12**, 3062 (2012)
11. N. Jain, T. Bansal, C. Durcan, and B. Yu, *IEEE Electron Device Lett.* **33**, 925 (2012)
12. Y. F. Wu, B. P. Keller, S. Keller, D. Kopolnek, P. Kozodoy, S. P. Denbaars, and U. K. Mishra, *Appl. Phys. Lett.* **69**, 1438 (1996)
13. V. Bougrov, M. E. Levinshtein, S. L. Rumyantsev, A. Zubrilov, in *Properties of Advanced Semiconductor Materials: GaN, AlN, InN, BN, SiC, SiGe*, edited by M. E. Levinshtein, S. L. Rumyantsev, and M. Shur (Wiley, New York, 2001), Chap. 1, pp. 1–30.

- <sup>14</sup>. J. Zou, D. Kotchetkov, A. A. Balandin, D. I. Florescu and Fred H. Pollak, *J. Appl. Phys.* **92**, 2534 (2002)
- <sup>15</sup>. R. J. Shul, G. A. Vawter, C. G. Willison, M. M. Bridges, J. W. Lee, S. J. Pearton, and C. R. Abernathy, *Solid-State Electron.* **42**, 2259 (1998).
- <sup>16</sup>. A. Watanabe, T. Takeuchi, K. Hirose, H. Amano, K. Hiramatsu, I. Akasaki, *J. Cryst. Growth* **128**, 391 (1993)
- <sup>17</sup>. A. Perez-Tomas, M. Placidi, X. Perpina, A. Constant, P. Godignon, X. Jorda, P. Nrosseland, And J. Millan, *J. Appl. Phys.* **105**, 114510 (2009)
- <sup>18</sup>. M. Esposito, S. Krishnamoorthy, D. Nath, S. Bajaj, T. Hung, and S. Rajan, *Appl. Phys. Lett.* **99**, 133503 (2011)
- <sup>19</sup>. A. Konar, T. Fang, and D. Jena, *Phys. Rev. B* **82**, 115452 (2010)
- <sup>20</sup>. T. Hung, M. Esposito, and S. Rajan, *Appl. Phys. Lett.* **99**, 162104 (2011)
- <sup>21</sup>. O. Mitrofanov and M. Manfra, *J. Appl. Phys.* **95**, 6414 (2004)

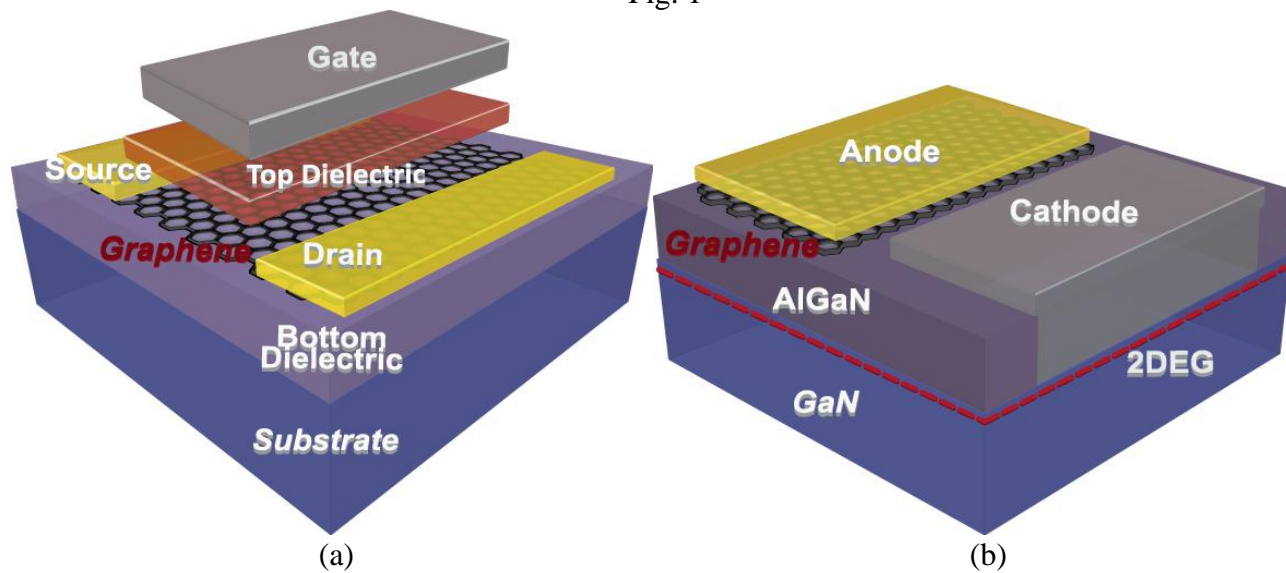
# Figures



(a)

(b)

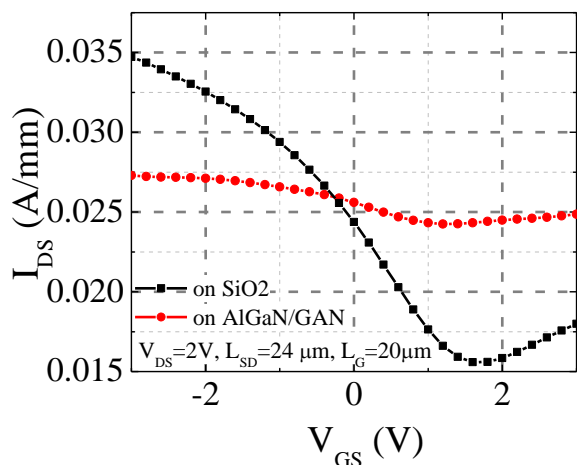
Fig. 1



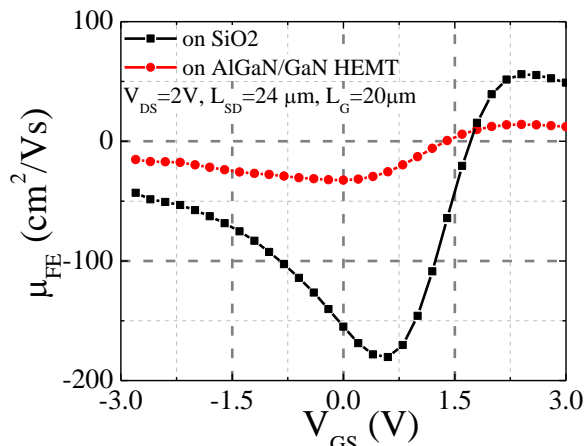
(a)

(b)

Fig.2



(a)



(b)

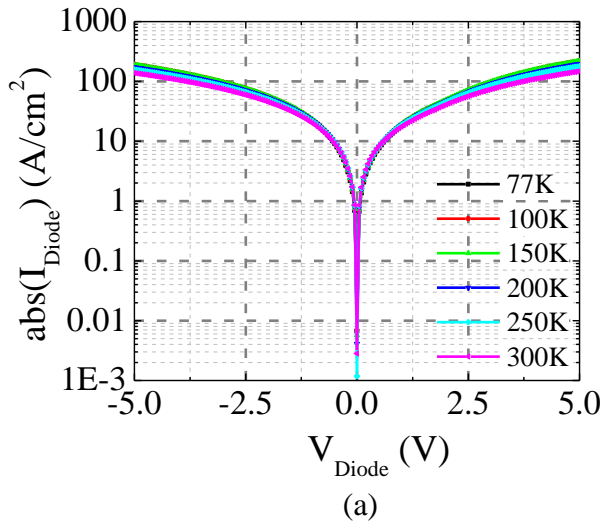


Fig. 3

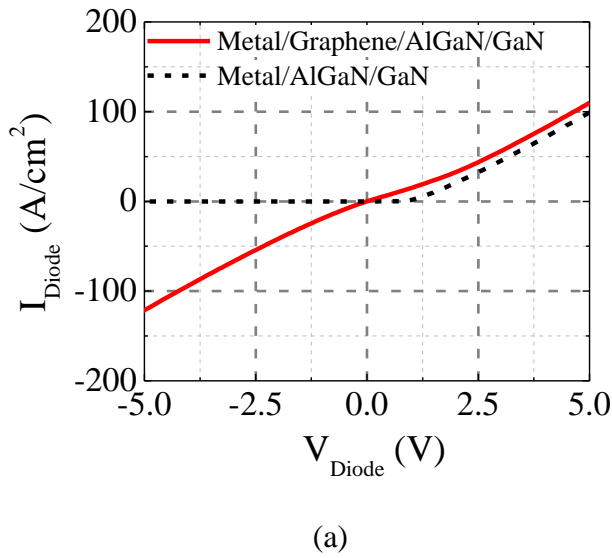
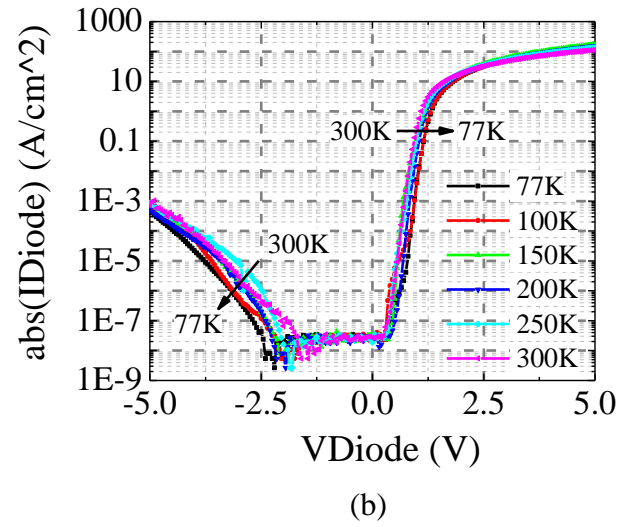


Fig.4

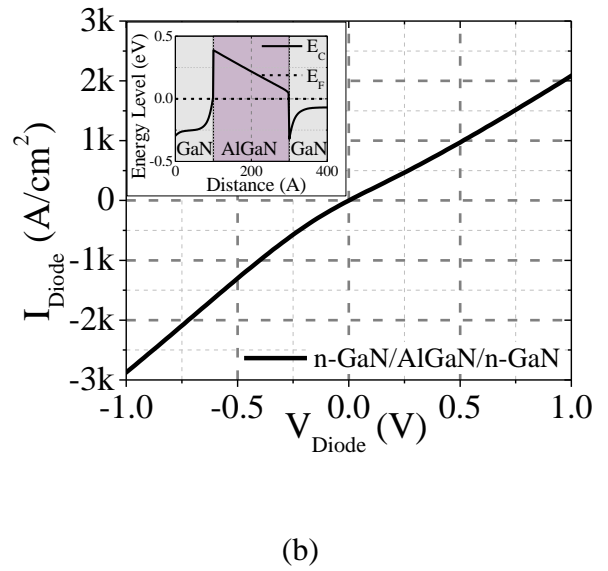


Fig.5

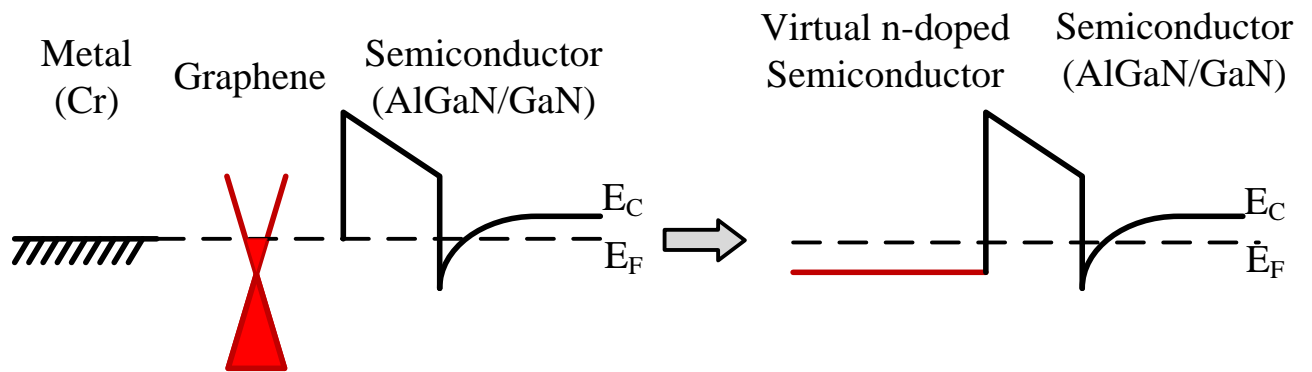


Fig.6

### **FIGURE LEGENDS:**

Figure 1: (a) the measured XRD (outset) and AFM (inset) data on AlGa<sub>N</sub>/Ga<sub>N</sub> substrate and (b) Raman spectra taken on transferred graphene on AlGa<sub>N</sub>/Ga<sub>N</sub> and SiO<sub>2</sub> substrates with the epitaxial structure of each substrate.

Figure 2: Schematic view of (a) a top-gated graphene FET and (b) a metal-graphene-semiconductor diode

Figure 3: (a) the measured transfer characteristics ( $I_{DS}$ - $V_{GS}$ ) of graphene FETs and (b) the extracted field-effect carrier mobility of the transistor.

Figure 4: Temperature dependent (77K -300K) Current-voltage (I-V) characteristics of (a) M-G-S junction and (b) M-S junction

Figure 5: Tunneling I-V characteristics in (a) M-(G)-S junction and (b) S-S (Ga<sub>N</sub>/AlGa<sub>N</sub>/Ga<sub>N</sub>) junction diodes

Figure 6: Proposed schematic band diagram of Metal-Graphene-AlGa<sub>N</sub>-Ga<sub>N</sub> junction